J Fluoresc (2011) 21:1431–1438
DOI 10.1007/s10895-010-0827-6

ORIGINAL PAPER

Photolumiscent Properties of Nanorods and Nanoplates $Y_2O_3:Eu^{3+}$

Ana Paula de Moura · Larissa Helena de Oliveira · Elaine Cristina Paris · Máximo Siu Li · Juan Andrés · José Arana Varela · Elson Longo · Ieda Lucia Viana Rosa

Received: 28 September 2010 / Accepted: 29 December 2010 / Published online: 15 January 2011

Abstract Nanorods and nanoplates of $Y_2O_3:Eu^{3+}$ powders were synthesized through the thermal decomposition of the $Y(OH)_3$ precursors using a microwave-hydrothermal method in a very short reaction time. These powders were analyzed by X-ray diffraction, field emission scanning electron microscopy, Fourrier transform Raman, as well as photoluminescence measurements. Based on these results, these materials presented nanoplates and nanorods morphologies. The broad emission band between 300 and 440 nm ascribed to the photoluminescence of Y_2O_3 matrix shifts as the procedure used in the microwave-hydrothermal assisted method changes in the $Y_2O_3:Eu^{3+}$ samples. The presence of Eu^{3+} and the hydrothermal treatment time are responsible for the band shifts in $Y_2O_3:Eu^{3+}$ powders, since in the pure Y_2O_3 matrix this behavior was not observed. $Y_2O_3:Eu^{3+}$ powders also show the characteristic Eu^{3+} emission lines at 580, 591, 610, 651 and 695 nm, when excited at 393 nm. The most intense band at 610 nm is responsible for the Eu^{3+} red emission in these materials, and the Eu^{3+} lifetime for this transition presented a slight increase as the time used in the microwave-hydrothermal assisted method increases.

Keywords Photoluminescence · Nanorods · Nanoplates · Yttrium oxide · Europium · Microwavehydrothermal method

A. P. de Moura · L. H. de Oliveira · E. C. Paris · I. L. V. Rosa (✉)
Departamento de Química, Universidade Federal de São Carlos, 13565-905 São Carlos, SP, Brazil
e-mail: ilvrosa@ufscar.br

J. A. Varela · E. Longo
Instituto de Química, Universidade Estadual Paulista, 14800-900 Araraquara, SP, Brazil

M. S. Li
Instituto de Física de São Carlos, USP, P.O. Box 369, 13560-970 São Carlos, SP, Brazil

J. Andrés
Departament de Química Física y Analítica, Universitat Jaume I, Castello de la Plana 12071, Spain

Introduction

Over the past decades there has been a growing interest in the preparation, characterization, and optimization of a variety of compounds doped with trivalent rare earth ions for the development of new or improved optoelectronic devices, which include solid state lasers, infrared optical fiber amplifiers, luminescent lamps, optical data storage, 3D displays, etc. [1–5].

Yttrium oxide (Y_2O_3) possesses excellent properties and it has many attractive applications such as laser and infrared optical materials [6–9]. Y_2O_3 is known through its use as the host of rare earth-doped, and, in particular europium (Eu^{3+})–doped Y_2O_3 luminescent presents high luminescence efficiency, high thermostability and chemical durability [2–4]. In addition, one of the most important properties for phosphors application is their chemical purity and low production costs [5]. Therefore, a variety of methods have been used to prepare Y_2O_3-based phosphors such as spray pyrolysis [10], chemical vapor deposition [11], sol–gel [12], and microwave-assisted [12] to render different kind of Y_2O_3 nanostructures, such as nanotubes [13], nanowires [14], nanorods [15] and nanobelts [16].

Since the determining work of Gedye1 in 1986, the use of microwaves has become a well established technique in chemistry that has found numerous applications in the laboratory as well as in industry [17–19]. Microwave heating is a versatile and widely used tool for preparative

chemistry and have continually demonstrated its worth within the laboratory setting. A number of books on microwave- assisted synthesis have been published recently [20–22]. The microwave-assisted heating is a greener approach to synthesize materials in a shorter time (from several minutes to a few hours) and with lower power consumption (hundreds of Watts) compared to the conventional heating at the same temperatures [23–27], as a consequence of directly and uniformly heating of the components, although other intriguing effects such as changing in the reaction selectivities and increase of reactional rates (microwave catalysis). Consequently, microwave synthesis is becoming quite common in several areas as material sciences, nanotechnology, inorganic, organic, biochemical, or pharmaceutical laboratories [10, 28–32].

Preparation of Y_2O_3:Eu^{3+} phosphors by the microwave-hydrothermal assisted method (MH) remains surprisingly scarce. Spherical particles of Y_2O_3 and Y_2O_3:Eu^{3+} was prepared using the MH method via hydrolysis in aqueous solution at high-temperature in the presence of urea, and the authors reported that the obtained materials present high crystallinity and high luminescence intensity. Cubic nanocrystalline Y_2O_3:Eu^{3+} with a spherical shape presenting 20–30 nm of diameters was successfully prepared using a novel approach, micro-emulsion microwave heating. The obtained materials were excited with 255 nm light, showing bright red emission due to the 4f-4f transitions of Eu^{3+} ions, and the highest photoluminescence (PL) intensity at 611 nm was determined in the sample containing about 6 mol% Eu^{3+} [12].

The present work reports on the PL behaviour of nanorods and nanoplates Y_2O_3:Eu^{3+} powders synthesized via a different MH method for first time here. We also analyzed the influence of the preparation time of the precursors on the optical and morphological properties of these materials, using X-ray diffraction (XRD), field emission microscopy (FEG-SEM), Ultraviolet–visible (UV–vis), absorption and Raman spectroscopy. The PL measurements of the Y_2O_3:Eu^{3+} have been employed on the basis of experimental analysis and it was observed interesting results. The origin of the PL emission excited in different wavelengths (394 and 350 nm) is therefore discussed here in details.

Experimental Procedures

Synthesis of the Precursors

The synthesis of the precursors was performed using the following procedure: A solution composed by 1.0 mmol of $Y(NO_3)_3.8H_2O$ and 80 mL of water were mixed and stirred for 30 min at room temperature. To this homogenous solution was then added 20 mL of 0.25 mmol of Eu_2O_3 diluted in HNO_3. The final pH value of 12.5 was adjusted using a 5.00 M NaOH solution. After stirring for about 30 min, the resulted mixture was transferred to a Teflon-lined stainless autoclave. This autoclave was then sealed and placed into a MH (2.45 GHz, maximum power of 800 W). The MH conditions were kept at 140 °C for 10, 20 and 40 min. The white powders, obtained through these different times, were labeled, respectively, as **P1**, **P2** and **P4**, collected, washed with water, and then dried at 60 °C for 8 h under atmospheric air in a conventional furnace.

Synthesis of Y_2O_3 and Y_2O_3:Eu^{3+} Powders

The Y_2O_3:Eu^{3+} powders were obtained from thermal decomposition of the precursors **P1**, **P2** and **P4.** These precursor powders were placed in ceramic crucibles and heated in a microwave sintering furnace at 500 °C for 20 min. These calcinated white powders were respectively called as **Y1**, **Y2** and **Y4** samples. The procedure used for the obtention of pure Y_2O_3 powders was the same as for Y_2O_3:Eu^{3+} powders, resulting in the samples **NY1**, **NY2** and **NY4**.

Characterization

Y1, **Y2** and **Y4** as well as **NY1**, **NY2** and **NY4** samples were characterized by powder X-ray diffraction using a Rigaku-DMax 2500PC, Japan, with Cu Kα radiation, λ= 1.540598 Å, in the 2θ range from 5 to 75° using an increment of 0.02°/min. The PL was measured with a Thermal Jarrel-Ash Monospec 27 monochromator and a Hamamatsu R446 photomultiplier. The 350.7 nm exciting wavelength of a krypton ion laser (Coherent Innova) was used, with the nominal output power of the laser power kept at 200 mW. All the measurements were taken at room temperature. The excitation and emission spectra of the Y_2O_3:Eu^{3+} samples were measured in a Jobin Yvon-Fluorolog 3 spectrofluorometer at room temperature using a 450 W xenon lamp as excitation energy source. Lifetime data of the Eu^{3+} $^5D_0 \rightarrow {}^7F_2$ transition in the Y_2O_3:Eu^{3+} samples were evaluated from the decay curves using the emission wavelength set at 612 nm and excitation wavelength set at 393 nm. The morphologies and sizes of the samples were observed using a field emission gun scanning electron microscopy (FEG-SEM) - Jeol JSM 6330F.

Results and Discussion

Figure 1(a) presents the XRD patterns of the precursors, represented by the sample **P1**, since **P2** and **P4** diffracto-

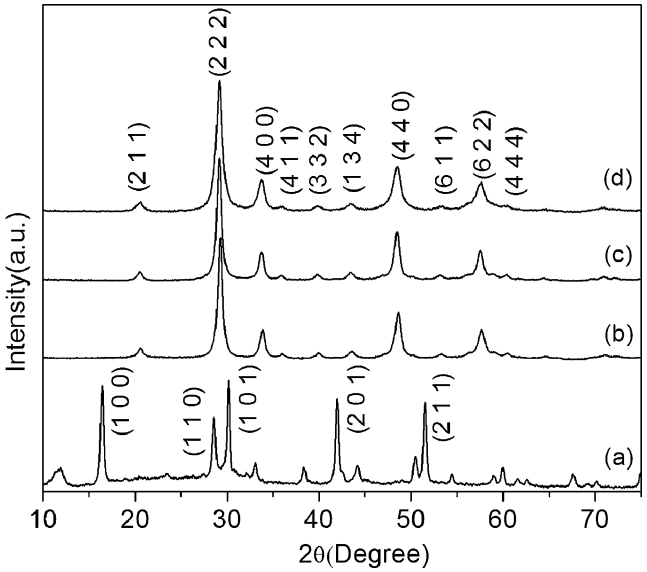

Fig. 1 XRD patterns of the as-prepared **P1** powder (**a**); and the Y_2O_3:Eu^{3+} powders heated at 500 °C for 20 min in a microwave oven (**b**) **Y1**, (**c**) **Y2** and (**d**) **Y4**

grams have the same feature. Figure 1(b, c and d) shows the XDR patterns of the Y_2O_3:Eu^{3+} powders, **Y1**, **Y2** and **Y4**, respectively. In the diffractogram of **P1** (Fig. 1(a)), it was not observed any diffraction peak ascribed to the Y_2O_3 crystalline phase. The precursor composition is mainly associated to yttrium hydroxide ($Y(OH)_3$). This conclusion was possible, since this diffractogram presents the characteristic peaks of this matrix according to JCPDS data file (# 83-2042). However, in the XDR patterns of the Y_2O_3:Eu^{3+} powders (Fig. 1(b, c and d)), was observed the diffraction peaks ascribed to a pure body-centered cubic Y_2O_3 phase at 2θ=20.5°, 29.1°, 33.8°, 36.1°, 39,9°, 43,5°, 48.6°, 53.3°, 57.7° and 60,5°, corresponding, respectively, to the (211), (222), (400), (411), (332), (134), (440), (611), (622) and (444), which are in accordance to the JCPDS # 43-1036. From these XDR patterns it was possible to noticed that a heat treatment of 500 °C for only 20 min under a microwave radiation is enable to result in a Yttrium oxide phase, so this is the advantage of this synthetic route, compared to another ones [33–35]. None peaks related to other phases were detected at Fig. 1(b, c and d). So, trough the RXD technique the products **Y1**, **Y2** and **Y4,** prepared by this method, are completely pure in terms of chemical composition.

The synthesis process was then accompanied by the emission and excitation spectra of the Eu^{3+} ion in the doped materials. These spectra data allows us a better understanding on the interactions around the Eu^{3+} ions than the X-ray technique, since RXD technique detects only the long-range interactions, while PL measurements is enable to give information on the Eu^{3+} interactions with the inorganic matrix in a short range distance. The excitation spectra of **Y1**, **Y2** and **Y4** samples are presented at Fig. 2. An analysis of the results shows that it was possible to observe narrow bands associated to the $4f^6$ intraconfigurational transitions from the $^7F_0$ ground state to the $^5G_6$ excited ones at 362 nm, $^5H_4$ at 382 nm, and $^5L_6$ at 394 nm, being the $^7F_0 \rightarrow {}^5L_6$ transition one of the most intense as it is normally noticed in inorganic matrix [36]. In this Fig. it was also noticed a broad absorption band that is observed in the range of 250–280 nm (not shown), which was ascribed to charge transfer from Y_2O_3 matrix to Eu^{3+} ions.

The PL emission spectra presented in Fig. 3(a, b, c) show the Eu3+ emission line ascribed to transitions from the Eu3+5D0 excited states to the ^7F_j (J=0, 1, 2, 3 and 4) fundamental ones in the **Y1**, **Y2** and **Y4** powders excited at 393 nm. The most intense band at 610 nm is due to the $^5D_0 \rightarrow {}^7F_2$ transition and is called as hypersensitive, being strongly dependent of the Eu^{3+} surrounding, since it is governed by the forced electric dipole mechanism. The emission spectra of all samples presented the Eu^{3+} $^5D_0 \rightarrow {}^7F_J$ (J=0, 1, 2, 3 and 4) transitions at 580, 591, 610, 651 and 695 nm, respectively. This indicates that Eu^{3+} site symmetry has no center of inversion. The band emission in the red region (610 nm) is predominant in the PL spectra. The feature of these spectra is similar to data reported in the literature for Eu^{3+} sites into the Y_2O_3 matrix. From the spectroscopic point of view, Eu^{3+} presents an intense red emission in inorganic systems having low symmetry, and normally is used as a probe due to its following characteristic properties (1) the excited states ^5D_J (J=0, 1, 2 and 3) are well separated (~12 000 cm^{-1}) from the ground terms ^7F_J' (J'=0, 1, 2, 3, 4, 5 and 6); (2) both $^5D_0$ main emitting level and $^7F_0$ ground state are non-degenerated leading to a single $^5D_0 \rightarrow {}^7F_0$ transition when

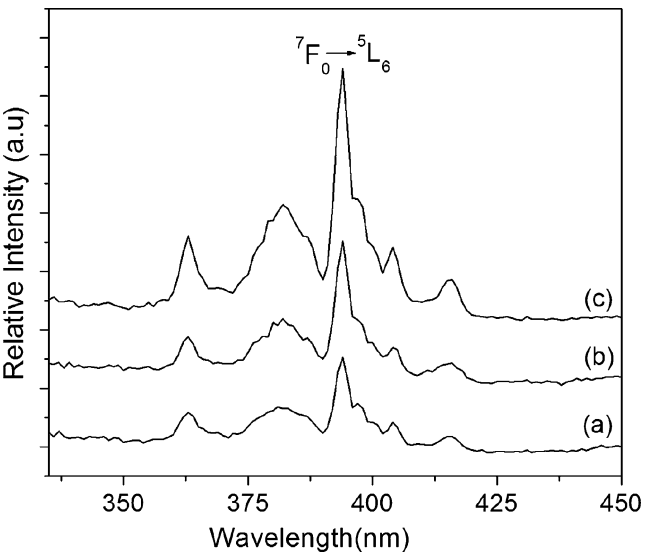

Fig. 2 Excitation spectra of Y_2O_3: Eu^{3+} powders heated at 500 °C for 20 min in a microwave oven (**a**) **Y1**, (**b**) **Y2** and (**c**) **Y4**

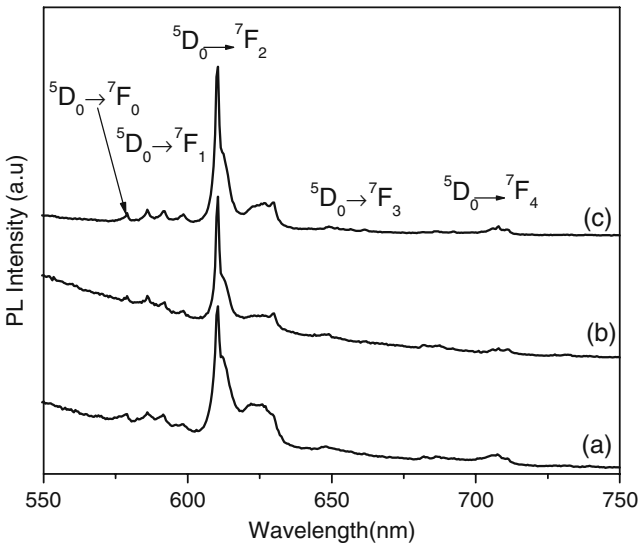

Fig. 3 Emission spectra of Y_2O_3: Eu^{3+} powders heated at 500 °C for 20 min in a microwave oven (**a**) $\mathbf{Y_1}$, (**b**) $\mathbf{Y_2}$ and (**c**) $\mathbf{Y_4}$. All samples were excited with a xenon lamp in 394 nm, at room temperature

the Eu^{3+} ions occupy C_s, C_n or C_{nv} site symmetries, therefore the $^5D_0 \rightarrow ^7F_0$ transition usually appears as a single peak in the photoluminescence spectra as the Eu^{3+} ions occupy identical site symmetries [37–40]. This fact facilitates the interpretation of the spectral data and provides informations on the eventual existence of more than one site symmetry occupied by the Eu^{3+} ion; (3) The $^5D_0 \rightarrow ^7F_1$ transition can be used as a reference transition because it is allowed by forced magnetic dipole, and consequently the intensity of this transition is not considerably altered by the Y_2O_3 matrix perturbing crystal field; (4) long luminescence decay time of around milliseconds for the $^5D_0$ level and (5) exceptionally large Stokes shifts when the emission spectra are obtained through the direct excitation of the Eu^{3+} $^5L_6$ level, at around 394 nm, like in this case (see Fig. 2), or through the excited state that is located at higher energies belonging to the host matrix or, in some cases, to organic ligands. The insert of Fig. 3 shows the photoluminescence spectrum of the precursor P1, as illustration, obtained at the same conditions as those at Fig. 3(a, b and c). As we can see, the P1 photoluminescence spectrum presents Eu^{3+} emission bands that were in accordance with the $Y(OH)_3$ Eu^{3+} doped [34].

It was noticed a decrease in the Eu^{3+} emission intensity when the samples were submitted to the microwave radiation from 10 to 20 min, indicating a structural rearrangement around Eu^{3+}. As the time of exposure to microwave radiation increases from 20 to 40 min, however, it was observed an increase in the relative intensity of the Eu^{3+} characteristic bands (Fig. 3(a, b and c)). During the sintering process the tendency to increase the emission intensity is due to the fact that OH^- groups around the Eu^{3+} are being replaced by the O^{2-} bonds of the Y_2O_3:Eu^{3+} matrix. OH^- groups have different vibration levels, whose energies are located between the $^5D_0$ excited level and the $^7F_6$ ground one of the Eu^{3+} ions in this framework. So, as these groups are substituted by the Eu^{3+} it is noticed the decrease in the emission quenching caused by the non-radiative processes decrease [41].

The decay curves of the Eu^{3+} $^5D_0 \rightarrow ^7F_2$ transition excited at 393 nm with the emission set at 613 nm, presented a non-exponential feature and when fitted in a bi-exponential function, resulted in lifetimes of 1.19 ms for **Y1,** 1.70 ms for **Y2** and 1.76 ms for the **Y4** sample, determined from the first part of the curves, respectively. As the time of heat treatment enhances, it was noticed an increase in the lifetime of the Eu^{3+} emission, indicating the incorporation of this ion by the Y_2O_3 matrix.

Raman spectroscopy can be used to characterize the phonon energy of these materials. The order–disorder degree in a short range of the crystalline structure was studied through the spectroscopic analysis. Figure 4(a, b and c) displays, respectively, the Raman spectra of Y_2O_3: Eu^{3+} powders **Y1**, **Y2** and **Y4** after heated at 500 °C for 20 min in the microwave oven. From these Raman spectra were verified the **Y1**, **Y2** and **Y4** samples presented the Raman active mode at 372, 461 and 583 cm^{-1}, which are related to the cubic Y_2O_3 phase according to recent report on [42, 43] Raman spectrum of Y_2O_3. These data are also in accordance to the XDR patterns. As the time of exposure to the microwave radiation increases the relative intensity of the Raman active modes enhances, indicating an increase in the degree of structural order at short-range.

To a better understanding of the PL properties and its dependence on the structural order–disorder in the Y_2O_3 lattice, the PL emission spectra of the Y_2O_3:Eu^{3+} powders

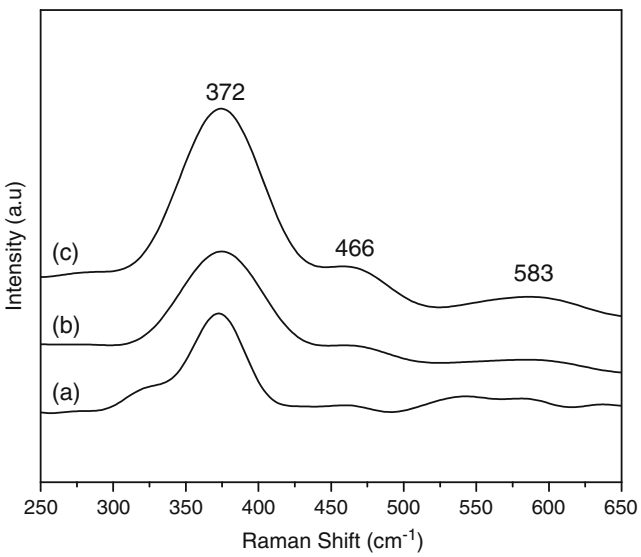

Fig. 4 RAMAN spectra of the **Y1**(**a**), **Y2**(**b**) and **Y4** (**c**) samples

Y1, **Y2** and **Y4** were performed at room temperature, using an excitation of a krypton laser source at 350.7 nm. These spectra are presented in Fig. 5a, where it was also observed a broad emission band ascribed to the emission of the Y_2O_3 matrix for all samples, as well as the characteristic bands of Eu^{3+} ions. In the PL spectrum of the **Y1** sample, the broad band is noticed from 300 to 440 nm, presenting an emission intensity maximum at 423 nm, while **Y2** sample presented a maximum at 429 nm (violet region). In the PL emission spectrum of the **Y4** sample, this broad band was shifted to a higher wavelength, with a maximum at 446 nm (blue region). This shift of the maximum intensity of the broad band can be associated to a larger charge density around Eu^{3+} compared to the Y^{3+} sites caused by the lanthanide contraction. The variation of the hydrothermal treatment time can modify the material surface promoting the appearing of deep defects in the Y_2O_3:Eu^{3+} matrix, which is also responsible for the broad band shift to higher wavelength (red region). The PL emission spectra of pure Y_2O_3 powders, N**Y1**, N**Y2** and N**Y4**, are presented in the Fig. 5b. These broad emission bands are due to charge transfer into the inorganic matrix, and no shift was observed with the microwave performance used in this study. In accordance with these results, it is clear that both the presence of Eu^{3+} and the hydrothermal treatment time are responsible for the band shifts, since in the samples N**Y1**, N**Y2** and N**Y4** (Fig. 5b) this behavior was not observed.

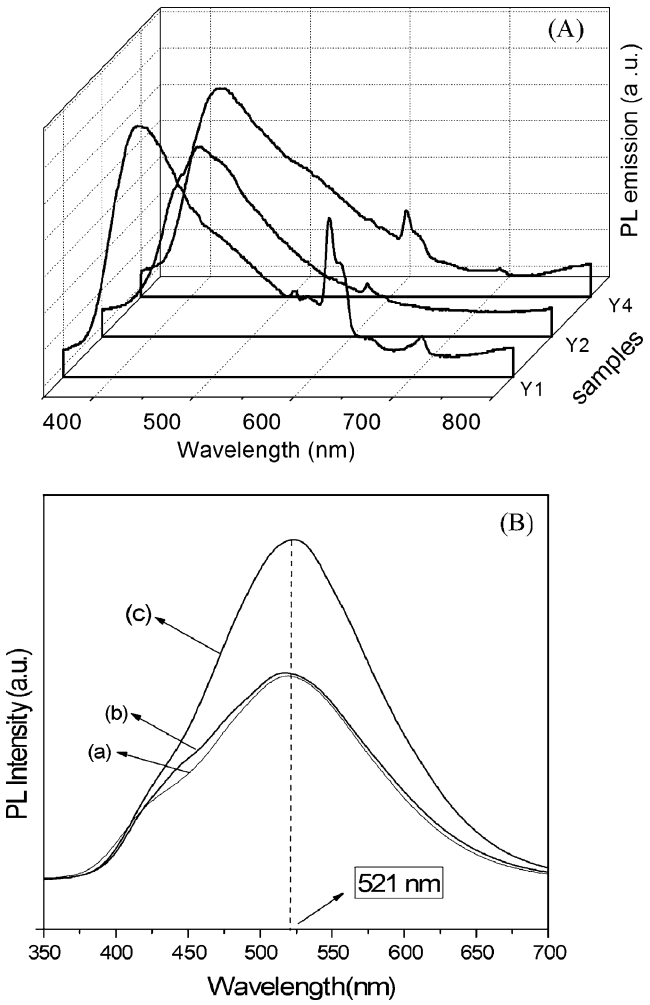

Fig. 5 (**A**) PL spectra of the Y_2O_3: Eu^{3+} powders microwave heated at 500 °C for 20 min for $\mathbf{Y_1}$, $\mathbf{Y_2}$ and $\mathbf{Y_4}$. (**B**) PL spectra of the Y_2O_3 samples heated at 500 °C for 20 min microwave oven (**a**) N$\mathbf{Y_1}$, (**b**) N$\mathbf{Y_2}$ and (**c**) N$\mathbf{Y_4}$. All samples were excited with krypton ion laser of 350.7 nm, at room temperature

Figure 6 shows the FEG-SEM micrographies of the **Y1** (A and B), **Y2**(C and D) and **Y3** (E and F) samples, respectively. From these micrographies, it was verified that the particles are agglomerated and polydispersed. These systems presented two categories of morphologies. Some particles are nanowires-like and some others are nanoplates-like, then this phenomenon can be associated with the exposure time under microwave radiation. It was also observed homogeneity in the sizes of **Y2,** which presented an average length of around 276–297 nm and an average width of 33–34 nm. The **Y1** sample presented an average length of 560–874 nm and an average width of 50 nm, while the **Y4** sample presented an average length of 178–184 nm and an average width of 28 nm, corroborating with a nanoscale range.

Into the Teflon autoclave, firstly, the microwave radiation interacts with the permanent dipole of the liquid phase. This interaction leads to a vibration on the charged particles or molecules, resulting in a rapid heating of the chemical solution, promoting, consequently, the formation of the $Y(OH)_3$ precursor particles in a quickly way. The increase of the temperature by the microwave radiation promotes the dissociation of some $Y(OH)_3$ particles in Y^{3+} and OH^- ions. However, the thermodynamic conditions and the electrostatic interactions between these ions favor the recrystallization process. Moreover, the microwave radiation is able to accelerate the solid particles to elevated velocities, leading to an increase of the interparticle collisions, inducing the effective fusion of these particles at the point of collision. These mechanisms are responsible for the fast nucleation of the Y_2O_3 grains, as well as the aggregation of several small particles [44]. This phenomenon was verified by the formation of aggregated particles in different morphologies, being some of them nanowires and others nanoplates-like, as observed at Fig. 6(a), after 10 min of microwave heating. As the reaction proceeds from 10 to 20 min, some amorphous particles are dissolved and are, after that, condensed beginning the appearance of ultrafine wires of Y_2O_3, presented at Fig. 7(c). After 40 min of microwave radiation exposure, it is supposed that occur the precursor recrystallization, and through this process we suggest the coalescence of the precursor particles, giving

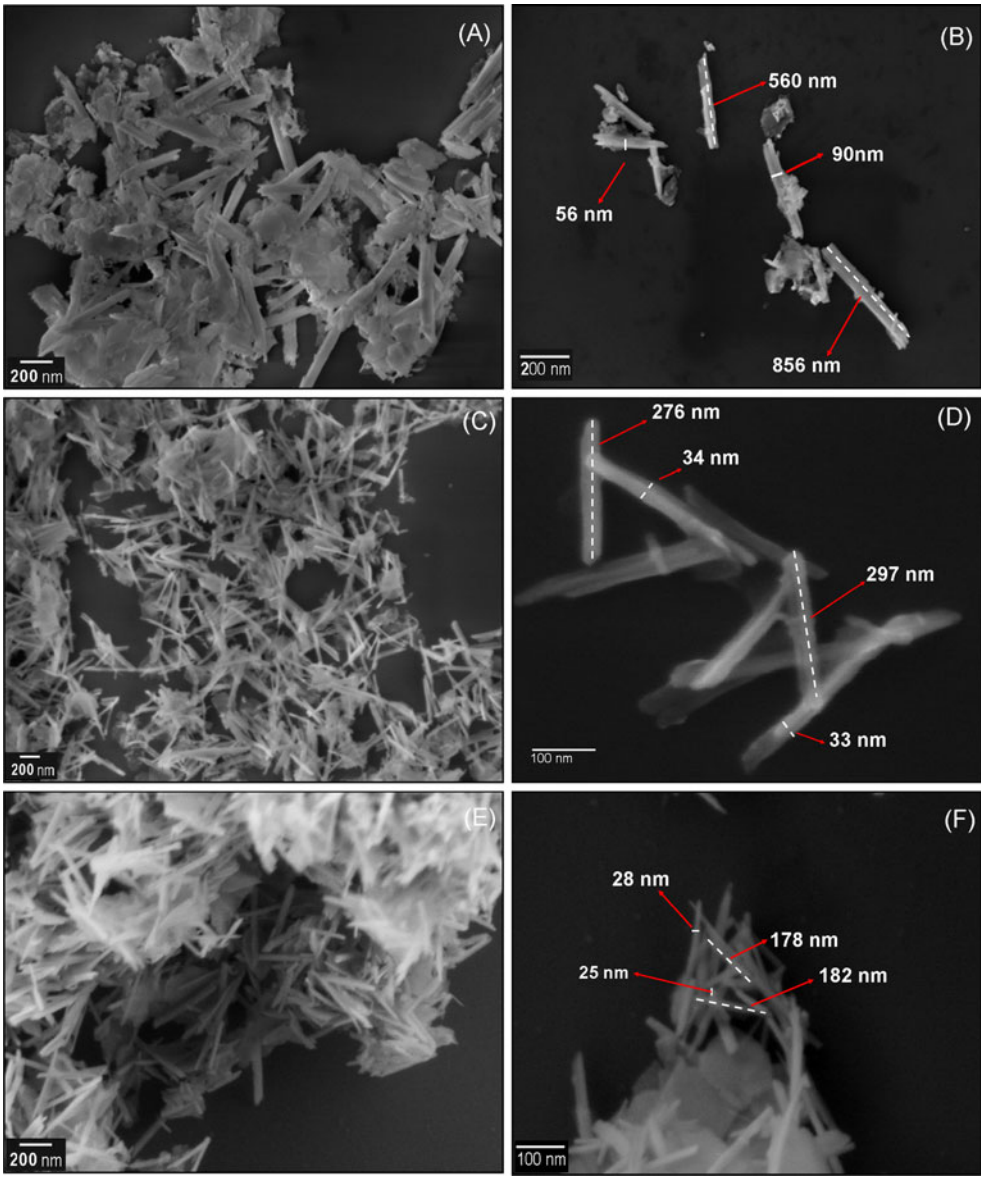

Fig. 6 FEG-SEM micrographies of Y_2O_3: Eu^{3+} of the powders heated at 500 °C for 20 min at microwave oven (**a** and **b**) $\mathbf{Y_1}$, (**c** and **d**) $\mathbf{Y_2}$ and (**e** and **f**) $\mathbf{Y_4}$

rise mainly to the Y_2O_3 phase (Fig. 6(e)). During the MH processing the reactional autoclave was not stirred. So, the electrostatic interactions between the ions increase, promoting aggregations that lead to the formation of Y_2O_3 seeds. It was also possible to observe, in this case, the presence of particles with two kinds of morphologies. The schematic representation of the growth mechanism of the Y_2O_3 particles by the MH proceeding is exposed at Fig. 7.

Conclusions

The synthesis process utilizing the MH method in a short time was successful in the obtention of the precursors giving rise to both pure and Eu^{3+} doped Y_2O_3. These materials presented two different kinds of morphologies, nanoplates and nanorods. The broad emission band be-

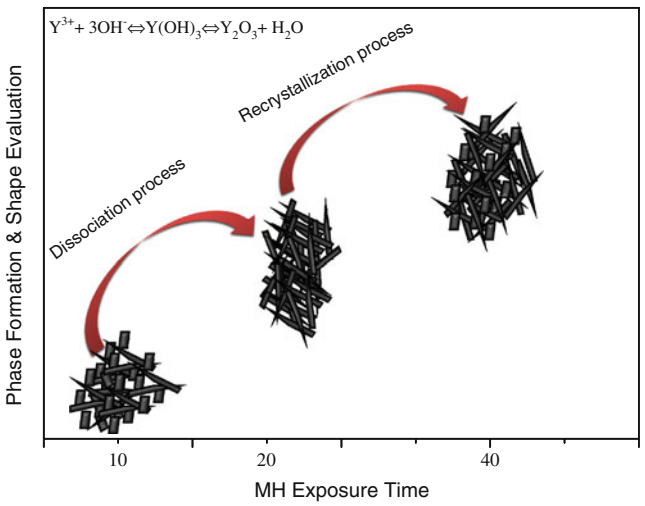

Fig. 7 Schematic representation of the growth mechanism of the Y_2O_3 particles by the MH method

tween 300 and 440 nm ascribed to the Y_2O_3 PL shifts as the MH procedure changes only in the Eu^{3+} doped materials. Y_2O_3:Eu^{3+} powders show the characteristics Eu^{3+} emission lines due to the $^5D_0$ to the ^7F_j (J=0, 1, 2, 3 and 4) transitions at 580, 591, 610, 651 and 695 nm, when were excited at 393 nm. The most intense band at 610 nm ($^5D_0 \rightarrow {}^7F_2$) is responsible for the Eu^{3+} red emission in these materials. The band emission in the red region (610 nm) is predominant in the PL emission spectra. From the spectroscopic point of view, Eu^{3+} ion gave us valuable information since it is a structural probe.

References

1. Ronda CR (1997) Recent achievements in research on phosphors for lamps and displays. J Lumin 72:49–54
2. Kitai AH (2003) Oxide phosphor and dielectric thin films for electroluminescent devices. Thin Solid Films 445:367–376
3. Wakefield BG, Holland E, Dobson PJ, Hutchison TL (2001) Luminescence properties of nanocrystalline Y_2O_3:Eu^{+3}. Adv Mater 13:1557–1560
4. Vanetsev AS, Butkina EP, Baranchikov AE, Shaporev AS, Dzuban AV, Soldatov MA, Hao Z, Tret'yakov YD (2009) Microwave-assisted synthesis of spherically shaped monodisperse Y_2O_3 and Y_2O_3:Eu powders. Dokl Chem 424:35–38
5. Serra OA, Cicillini SA, Ishiki RR (2000) A new procedure to obtain Eu^{+3} doped oxide and oxosalt phosphors. J Alloy Comp 303:316
6. Ikegami T, Li J-G, Mori T, Moriyoshi Y (2002) Fabrication of transparent Yttria ceramics by the low-temperature synthesis of Yttrium hydroxide. J Am Ceram Soc 85(7):1725–1729
7. Zheng JX, Ceder G, Maxisch T, Chim WK, Choi WK (2006) Factors determining the shape of the temperature dependence of the spontaneous magnetization of a ferromagnet. Phys Rev B 73:104101
8. Zhang J, An L, Liu M, Shimai S, Wang S (2009) Sintering of Yb^{3+}: Y_2O_3 transparent ceramics in hydrogen atmosphere. J Eur Ceram Soc 29:305–309
9. Jollet F, Noguera C, Thromat N, Gautier M, Duraud JP (1990) Electronic structure of Yttrium oxide. Phys Rev B 42(12):7587
10. Sun LD, Yao J, Liu C, Liao C, Yan CH (2000) Rare earth activated nanosized oxide phosphors: synthesis and optical properties. J Lumin 87–89:447–450
11. Lee MH, Oh SG, Yi SC (2000) Preparation of Eu-Doped Y_2O_3 luminescent nanoparticles in nonionic reverse microemulsions. J Colloid Interface Sci 226:65–70
12. Wu GS, Lin Y, Yuan XY, Xie T, Cheng BC, Zhang LD (2004) A novel synthesis route to Y2O3:Eu nanotubes. Nanotechnology 15:568–571
13. Zhang JL, Hong GY (2004) Preparation and characterization of the Y(2)O(3): Eu 3+ nanowires. Chem J Chin Univ-Chinese 25 (8):1416–1418
14. Li Q, Feng C, Jiao Q, Guo L, Liu C, Xu HB (2004) Shape-controlled synthesis of yttria nanocrystals under hydrothermal conditions. Phys Status Solidi, A 201(14):3055–3059
15. He Y, Tian Y, Zhu Y (2003) Large-scale synthesis of luminescent Y_2O_3:Eu nanobelts. Chem Lett 32(5):862–863
16. Whitefield PS, Davidson IJ (2000) Microwave synthesis of Li1025Mn1.975O4 and Li1+xMn2-xO4-yFy (x=0.05, 0.15; y= 0.05, 0.1). J Electrochem Soc 147(12):4476–4484
17. Gedye R, Smith F, Westaway K, Ali H, Baldisera L, Laberge L, Rousell J (1986) The use of microwave ovens for rapid organic synthesis. Tetrahedron Lett 27:279–282
18. Larhed M, Moberg C, Hallberg A (2002) Microwave-accelerated homogeneous catalysis in organic chemistry. Acc Chem Res 35:717–727
19. Kingston HM, Haswell JS (1997) Microwave-enhanced chemistry. American Chemical Society, Washington
20. Loupy A (ed) (2006) Microwaves in organic synthesis, 2nd edn. Wiley-VCH, Weinheim
21. Kappe CO, Stadler A (2005) Microwaves in organic and medicinal chemistry. Wiley-VCH, Weinheim
22. Lidström P, Tierney JP (eds) (2005) Microwave-assisted organic synthesis. Blackwell, Oxford
23. Bohr H, Bohr J (2000) Microwave-enhanced folding and denaturation of globular proteins. Phys Rev E 61(4):4310–4314
24. Blanco C, Auerbach SM (2002) Microwave-driven zeolite-guest systems show athermal effects from nonequilibrium molecular dynamics. J Am Chem Soc 2002(124):6250
25. Favretto L, Nugent WA, Licini G (2002) Tetrahedron Lett 43:2581–2584
26. Hoz ADL, Diaz-Ortiz A, Moreno A (2004) Selectivity in organic synthesis under microwave irradiation. Curr Org Chem 8 (10):903–918
27. Bren M, Janezic D, Bren U (2010) Microwave catalysis revisited: an analytical solution. J Phys Chem A 114:4197–4202
28. Kappe CO, Stadler A (2005) Microwaves in organic and medicinal chemistry. Wiley, Weinheim
29. Obermayer D, Gutmann B, Kappe CO (2009) Microwave chemistry in silicon carbide reaction vials: separating thermal from nonthermal effects. Angew Chem Int Ed 48(44):8321–8324
30. Yao BD, Wang N (2001) Carbon nanotube arrays prepared by MWCVD. J Phys Chem B 105:11395–11398
31. Zhu Y-J, Wang W-W, Qi R-J, Hu X-L (2004) Microwave – assisted synthesis of single-crystalline tellurium nanorods and nanowires in ionic liquids. Angew Chem Int Ed 43(11):1410–1414
32. Tompsett GA, Conner WC, Yngvesson KS (2006) Chem Phys Chem 7:29
33. Zhong S, Wang S, Huaping Xu, Hou H, Wen Z, Li P, Wang S, Rong X (2009) Spindlelike Y_2O_3:Eu^{3+} nanorod bundles: hydrothermal synthesis and photoluminescence properties. J Mater Sci 44(14):3687–3693
34. Wu X, Tao Y, Gao F, Dong L, Hu Z (2005) Preparation and photoluminescence of yttrium hydroxide and yttrium oxide doped with europium nanowires. J Cryst Growth 277(1–4):643–649
35. Wan J, Wang Z, Chen X, Li Mu, Qian Y (2005) Shape-tailored photoluminescent intensity of red phosphor Y_2O_3:Eu^{3+}. J Cryst Growth 284:538–543
36. Teotonio EES, Felinto MCFC, Brito HF, Malta OL, Trindade AC, Najjar R, Strek W (2004) Synthesis crystalline structure and photoluminescence investigations of the new trivalent rare earth complexes (Sm^{3+}, Eu^{3+} and Tb^{3+}) containing 2-thiophenecarboxylate as sensitizer. Inorg Chim Acta 357:451–460
37. Rosa ILV, Oliveira LH, Suzuki CK, Varela JA, Leite ER, Longo E (2008) SiO_2–GeO_2 soot preform as a core for Eu_2O_3 nanocoating: synthesis and photophysical study. J Fluoresc 18:541–545
38. Volanti DP, Rosa ILV, Paris EC, Paskocimas CA, Pizani PS, Varela JA, Longo E (2009) The role of the Eu3+ ions in structure and photoluminescente properties of $SrBI_2nB_2O_9$ powders. 31 (6):995–999
39. Buono-Core GF, Li H, Marciniak B (1990) Quenching of excited states by lanthanide ions and chelates in solution. Coord Chem Rev 99:55–87
40. Malta OL Brito HF, Menezes JFS, Gonçalves FR, Silva Alves S Jr, Farias FS Jr, de Andrade AVM (1997) Spectroscopic properties of a new light converting device Eu(thenoyltrifluoroacetonate), 2 (dibenzyl sulfoxide). A theoretical analysis based on structural data obtained from a sparkle model. J Lumin 75:255–268

41. Serra OA, Nassar EJ, Zapparolli G, Rosa ILV (1994) Organic complexes of Eu^{3+} supported in functionalized silica gel: highly luminescent material. J Alloys Compd 207–208:454–456
42. Ubaldini A, Carnasciali MM (2008) Raman characterisation of powder of cubic RE_2O_3 (RE=Nd, Gd, Dy, Tm, and Lu), Sc_2O_3 and Y_2O_3. J Alloy Comp 454:374–378
43. Guo H, Qiao YM (2009) Preparation, characterization, and strong upconversion of monodisperse Y2O3:Er3+, Yb3+ microspheres. Opt Mater 31(4):583–589
44. Sczancoski JC, Cavalcante LS, Joya MR, Espinosa JWN, Pizani PS, Varela JA, Longo E (2009) Synthesis, growth process and photoluminescent properties of $SrWO_4$ powders. J Colloid Interface Sci 330(1):227–236